Global active control of energy density in a mock tractor cabin

Benjamin M. Faber[a] and Scott D. Sommerfeldt[b]

(Received 2005 October 12; revised 2006 March 01; accepted 2006 March 10)

Low frequency tonal noise, associated with engine firing frequency, often makes a significant contribution to sound levels that exist inside tractor cabins. Because these tones are low frequency in nature, they present a considerable challenge to passive noise control techniques, but are good candidates for active noise control applications. The presence of such noise can also threaten machinery operators' auditory health in addition to posing a challenge to machinery manufacturers in their efforts to produce machines that meet standards for operator exposure to noise. Active minimization of acoustic energy density has been applied to a mock tractor cabin, targeting engine firing frequency in simulated static and dynamic machine conditions. Previous work has demonstrated that active control of energy density generally provides good global control of enclosed sound fields. Multiple microphones were distributed throughout the cab to verify the global nature of the control. Generated sinusoids as well as actual recorded tractor noise were used to simulate the uncontrolled acoustic field. Both static and dynamic results will be presented, showing the local attenuation at the error sensor and the global attenuation throughout the cab. © ***Institute of Noise Control Engineering***

Primary subject classification: 38.2; Secondary subject classification: 12.2

1 INTRODUCTION

Significant motivations exist for noise reduction in heavy equipment cabins. The noisy environments often encountered in heavy equipment cabins pose a risk to the health and safety of machinery operators, due in part to the amount of time operators spend in such environments.[1,2] Auditory fatigue and discomfort could potentially be reduced and mental concentration and job efficiency increased through the reduction of operator noise exposure. The need for equipment manufacturers to meet existing and future standards for operator exposure to noise presents another reason for the employment of relevant technology in the reduction of noise inside equipment cabs.

Prior investigation of noise in tractor cabins showed that discrete tones that are harmonically related to the rotation speed of the tractor's engine generally dominate the noise spectrum.[1-5] The tonal components of the engine noise make good candidates for active noise control (ANC), because of their relatively low frequencies. The low frequencies also make engine noise difficult to control through passive techniques, which could potentially add to the appeal of ANC from the perspective of equipment manufacturers.

ANC efforts in the past demonstrated the successful attenuation of engine tonal noise inside tractor cabins, but significant weaknesses of the control systems rendered them impractical for commercial installation. Noise reduction tended to be limited to a relatively small spatial region near the operator's head and error sensors were sometimes placed in locations that would be inconvenient for the operator. The inability of such control systems to adequately track rapid changes in tractor engine speed during normal work cycles was an additional drawback.[1-4] The approach taken by these systems was to minimize squared acoustic pressure (SP) at one or more error sensor locations.

The minimization of acoustic energy density (ED) by ANC systems can have certain advantages over the minimization of SP.[6-9] Acoustic ED depends on acoustic particle velocity in addition to acoustic pressure, which allows more information to be utilized by an ANC system that uses ED as a squared error signal. The additional dependence on particle velocity results in a more global control of an enclosed sound field than is often achieved through the minimization of SP alone. Additionally, an ED error sensor has a much lower probability of being placed in a nodal region than an SP sensor for the natural modes of the same enclosure.[9]

The potential advantages of an ED-based control system make it an attractive option for the reduction of low-frequency engine tones in closed tractor cabs. This paper discusses an ED-based ANC system, constructed at Brigham Young University, and the performance of the system in a simulated tractor cabin using synthesized tonal noise as well as recorded noise from an actual tractor.

2 THE CONTROL SYSTEM

2.1 An Energy-Based Error Sensor

Since acoustic ED is a sum of kinetic energy density, which is proportional to the square of particle velocity, and potential energy density, which is proportional to the square of acoustic pressure, its instantaneous value may be obtained by measuring particle velocity and pressure at a point. The dependence of the total instantaneous acoustic ED on particle velocity and pressure is given by:

$$e_i = \frac{1}{2}\rho_0\left[u^2 + \left(\frac{p}{\rho_0 c}\right)^2\right], \tag{1}$$

[a] *Department of Physics and Astronomy, N283 ESC, Brigham Young University, Provo, UT 84602; email:benfaber@byu.edu.*

[b] *Department of Physics and Astronomy, N283 ESC, Brigham Young University, Provo, UT 84602; email: scott_sommerfeldt@byu.edu*

where u^2, p, ρ_0, and c represent the magnitude squared of the acoustic particle velocity vector, the acoustic pressure, the ambient fluid density, and the speed of sound, respectively. By assuming the density of air and the speed of sound in air to be constant and known, the measurement of acoustic ED only requires that the particle velocity and pressure be obtained.

A two-microphone measurement technique allows one directional component of the particle velocity vector to be obtained in the direction defined by the location of the microphones. By embedding three orthogonally arranged pairs of microphones in a solid sphere, a three-dimensional particle velocity vector can be obtained for the point corresponding to the center of the sphere. The two-microphone technique assumes that some distance, d, separates the microphones and that no obstruction exists between them. However, the bias errors in the measurement due to the presence of a sphere turn out to be beneficial.[10] A spherical sensor with diameter d will behave similarly to a sensor with no obstruction between the microphones, but a microphone separation distance of $1.5d$. This allows a spherical sensor to be constructed two-thirds the size of a sensor with no sphere without any loss in accuracy. The performance of a wooden spherical ED sensor with a two-inch diameter and three pairs of inexpensive electret microphones was described by Parkins, *et al.*[8] The wooden sensor was shown to exhibit total energy density errors within ±1.75 dB in the frequency range $110 < f < 400$ Hz. Microphone configurations other than the three orthogonal pairs are possible for energy density sensors and some alternatives have been explored at Brigham Young University.[11]

2.2 The Algorithm

The well-known filtered-x LMS adaptive filtering algorithm provides a basis for the algorithm employed in the ED-based ANC system. However, the filtered-x algorithm had to be modified in order to minimize acoustic ED and the resultant algorithm is that described in greater detail by Sommerfeldt and Nashif.[7] Four control path transfer functions are required in order to produce four of the so-called filtered-x signals. These four transfer functions are obtained via an offline system identification algorithm for the pressure path as well as each of the paths corresponding to the three components of the particle velocity vector. The reference input signal, $x(n)$, is filtered by each of the four control path transfer functions to produce the filtered-x signals, $r_p(n)$, $r_{ux}(n)$, $r_{uy}(n)$, and $r_{uz}(n)$. In order to verify proper identification of the secondary paths within the DSP, the secondary path filters actually used by the control system were compared to high-resolution measurements of the same transfer functions. The high-resolution measurements were obtained at much higher sample rates, using longer time records. Fast and stable convergence of the control system occurred when enough filter coefficients were used in the DSP to capture more than 95% of the energy contained in the high-resolution impulse response.

The update equation for the vector of control filter coefficients, $\mathbf{w}$, at time n, is given as:

$$\mathbf{w}_{n+1} = \mathbf{w}_n - \mu\left(\frac{p(n)}{\rho_0 c^2}\mathbf{r}_p(n) - \sum_{m=1}^{3}\frac{u_m(n)}{\Delta x_m}\mathbf{r}_{um}(n)\right), \qquad (2)$$

where $u_m(n)$ is the m^{th} component of the instantaneous particle velocity at time n (m=1, 2, and 3 corresponds to the x, y, and z directions, respectively), and $\mathbf{r}_p(n)$ and $\mathbf{r}_{um}(n)$ are vectors containing the current (time n) and past values of the four filtered-x signals. Since the current system employs a two-microphone technique for the estimation of particle velocity, Δx_m represents the effective microphone separation distance in each of the three orthogonal directions and $p(n)$ is the instantaneous pressure averaged over all microphones. The energy-based algorithm's dependence on four error signals, pressure and three velocity components, makes it comparable to a four-channel version of the common filtered-x algorithm used for the reduction of squared acoustic pressure, although for ED control the error signals are colocated. The same stability criterion holds for the two algorithms.

Numerical simulations of ED control within a rectangular enclosure were reported by Parkins, *et al.*[6]

2.3 Control System Electronics

A 32-bit Texas Instruments DSP processor, capable of performing 120 million floating point instructions per second, provided more than enough processing power for the ED-based, feedforward adaptive algorithm. Analog-to-digital and digital-to-analog conversions were accomplished with the use of 12-bit converters. Because the control system only targeted low-frequency noise, all analog input and output signals were low-pass filtered using fourth order Butterworth filters with a cutoff frequency of 400 Hz. The system was generally operated with a sampling rate of 2 kHz, so the filters were sufficient to avoid any problems with aliasing. The hardware allowed for two control signals to be routed to the loudspeakers used as control actuators. Before passing through a power amplifier and on to the loudspeakers, the control signals passed through a crossover circuit in order to route frequencies less than 90 Hz to a subwoofer and frequencies greater than 90 Hz to one of two smaller satellite speakers. Each of the two control signals was routed to one of the satellite speakers, but the two signals were summed to produce the final control signal sent to the subwoofer.

3 EXPERIMENTAL SETUP

In an effort to simulate the use of an ED-based ANC system in a real tractor cabin, the control system was operated in a mock cabin consisting of a steel frame and 3/8-inch plywood panels on all sides except the front panel, which was made of 1/8-inch Plexiglas®. The frame measured 1.5 meters high and 1 meter wide. The length of the frame was 1.2 meters at the bottom and 1 meter at the top, so that the front panel (resembling a windshield) was sloped. A chair was placed in the back of the cab, centered between the two sides, on which a person could sit to simulate the presence of an equipment operator during measurements or to operate the ANC system from within the cab. Photos of the cab appear in Fig. 1. Numerically computed mode shapes for the first four modes of the cab, up to 200 Hz, are shown in Figs. 2 through 5. These mode shapes were obtained with the Finite Element Method using LMS SYSNOISE and assuming rigid boundaries.

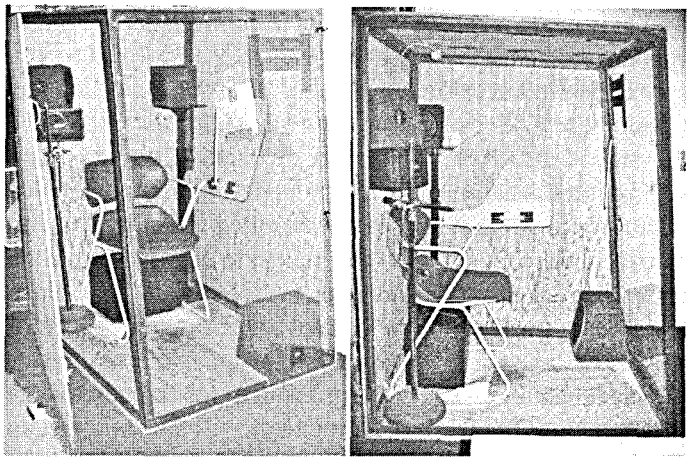

Fig. 1. Mock cabin photos. Front and side views on the left and right, respectively.

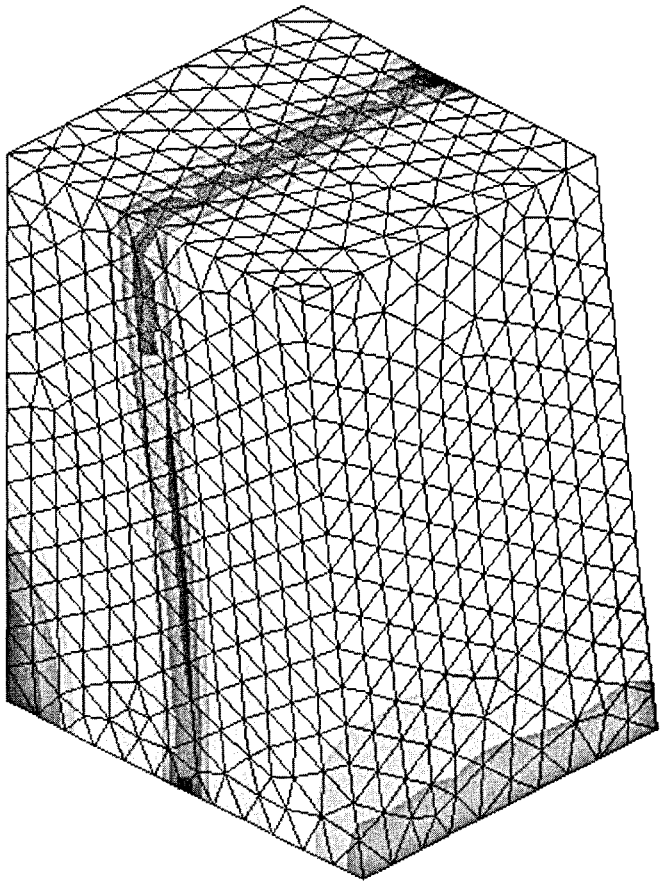

Fig. 3. The second cab mode at 154.0 Hz exhibits a single nodal plane dividing the front and back halves of the cab.

Uncontrolled noise was produced in the cab using a Mackie HR824 loudspeaker (the source speaker) with reasonably flat frequency response down to 37 Hz. The source speaker was placed underneath the chair inside the mock cab. The two satellite control speakers were positioned near the top corners of the mock cab in order to be near the operator's head, as well as to be in a position to couple well with the acoustic modes of the cab. The subwoofer was placed in the front left corner of the cab on the floor. The control speaker locations can be seen in the photos in Fig. 1. The error sensor was located directly above the operator's head. The benefit of this error sensor placement is that it enables the center of the so-called "zone of silence" to be as close as possible to the operators ears, while keeping the sensor out of the operator's way. Since the operator of a tractor will generally be centered between the two side walls of the cab, this placement would be more problematic for a simple pressure sensor. The potential presence of axial modes possessing nodal regions centered between the two side walls suggests that a pressure sensor should be placed to one side of the operator's head (see Fig. 4). An ED sensor, however, will only encounter an ED node where two or more pressure nodes overlap, which could not happen at the chosen error sensor location in the 0 to 200 Hz range of the mock cabin.

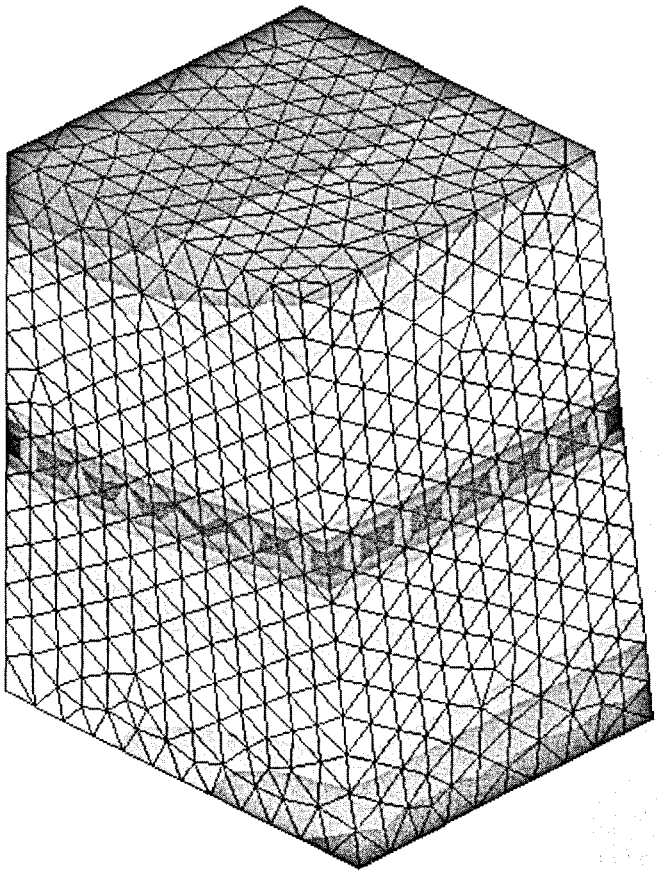

Fig. 2. The first cab mode at 113.2 Hz exhibits a single nodal plane dividing the top and bottom halves of the cab.

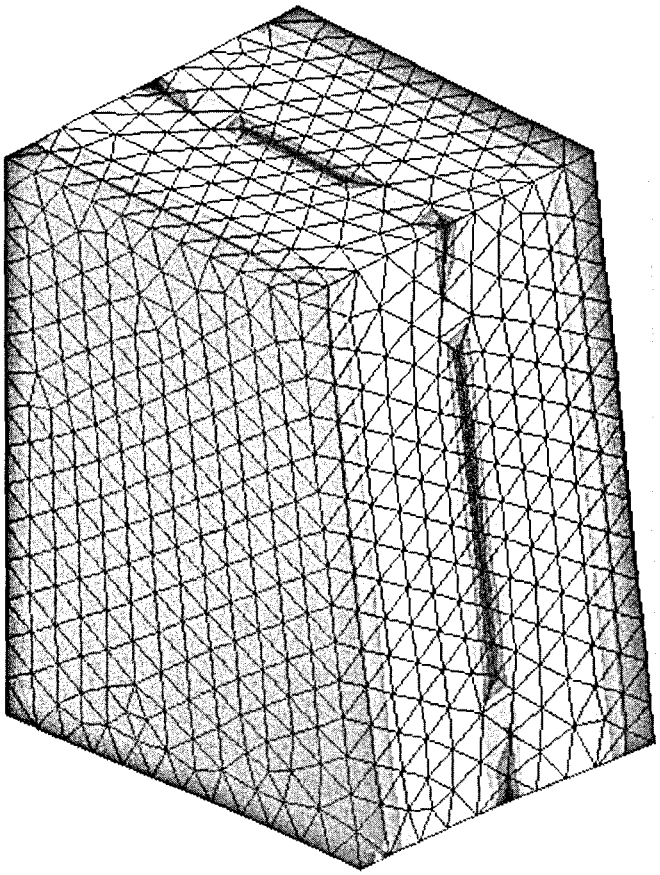

Fig. 4. The third cab mode at 170.8 Hz exhibits a single nodal plane dividing the right and left halves of the cab.

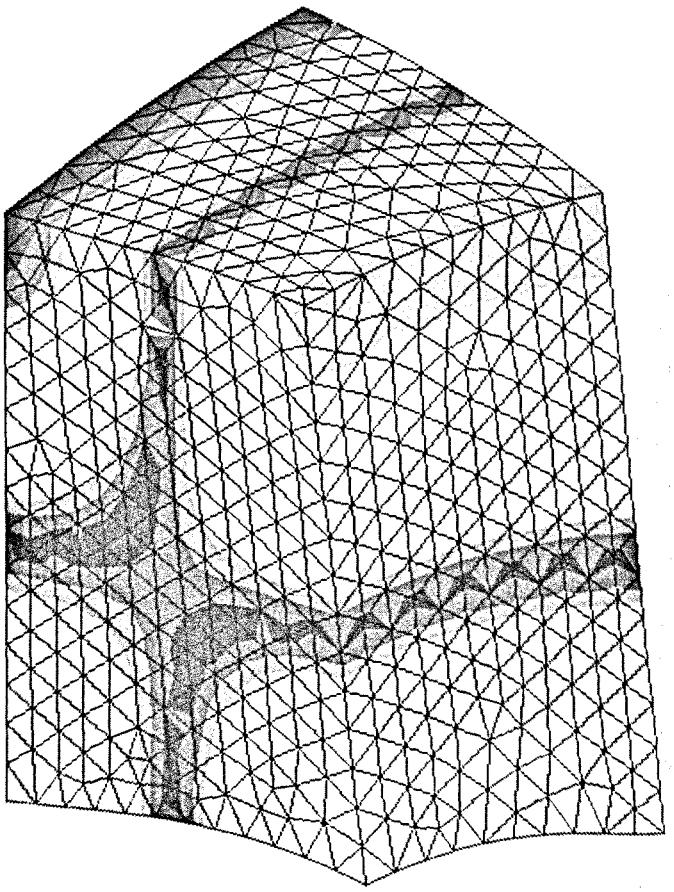

Fig. 5. The fourth cab mode at 194.8 Hz exhibits two intersecting nodal planes.

For measurements in which the uncontrolled noise was a synthesized sinusoid, the same signal was sent to the source speaker as well as to the reference input of the control system electronics. The tractor noise recordings, however, had two channels—one for the noise inside the cab, and the other for a tachometer signal from the tractor's engine. When the recorded tractor noise was used as the uncontrolled noise in the mock cab, the tractor noise signal was routed to the source speaker under the seat and the recorded tachometer signal was routed to the reference input of the control system electronics.

Fifteen microphones measured the sound pressure inside the mock cab in order to determine the global nature of the noise control. Twelve of these microphones were arranged in two parallel horizontal planes, above and below the height of the operator's ears. Two other microphones were strapped to a set of headphones to measure the sound pressure levels near the operator's ears. These headphones were sometimes worn by a person sitting inside the cab and sometimes suspended from the ceiling of the cab for measurements without a person in the cab. One additional microphone was used to measure the sound pressure at the error sensor location. Fig. 6 shows the placement of the microphones.

4 MEASUREMENTS

Both static (fixed frequency) and dynamic (swept frequency) sinusoids served as uncontrolled noise signals inside the mock cab to help quantify the performance of the ED-based ANC system. Static sinusoids were synthesized with several different frequencies ranging between 40 and 200 Hz, to test the control system at or near modal frequencies of the cab as well as away from modal frequencies. The chosen frequencies, for which results are discussed in the next section, are 50, 80, 113, 125, 154, 171, and 195 Hz. A dynamic excitation signal was created to explore the tracking abilities of

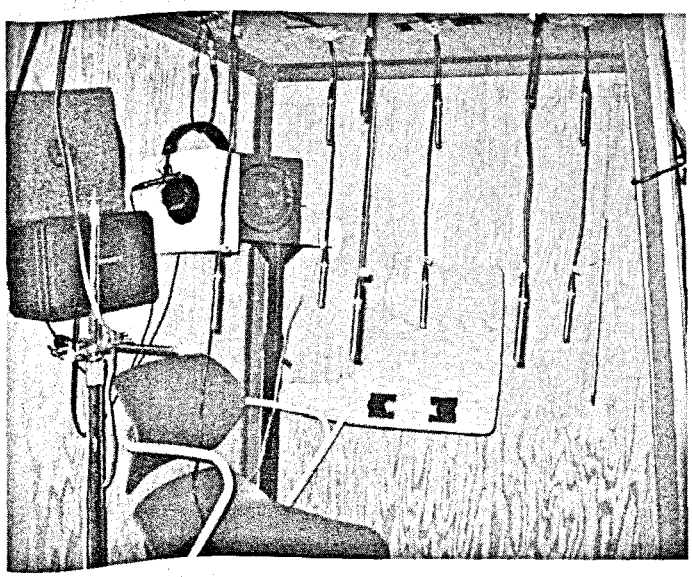

Fig. 6. Microphones used to measure the performance of the ANC

the ANC system. This dynamic signal was composed of four different sections. The frequency of the sinusoid was swept at a linear rate between 40 Hz and 200 Hz at two different rates. The slower sweeps had a duration of four seconds while the faster sweeps had a duration of one second. For portions of the test signal, the end frequencies were held for the same duration as the corresponding sweeps. A spectrogram of the dynamic noise signal can be seen in Fig. 7.

In order to more closely simulate the use of the ANC system in an actual tractor cab, static and dynamic engine noise was recorded inside a tractor cab along with a tachometer signal to be used for the reference input to the adaptive control algorithm. Static engine noise was recorded at engine speeds of approximately 820, 1800, 2000, and 2340 rpm, which produced dominant engine tones at 41, 91, 99, and 117 Hz. The dominant tones correspond to the engine firing frequency, which is three times the engine rotation frequency for a typical six-cylinder diesel engine. Additional recordings were made of the tractor engine noise as the engine speed was swept up and down between idle and full-throttle. Three different sweep rates were recorded, with the faster two corresponding to roughly the same sweep rates as the synthesized swept sine signal.

For all measurements reported in this paper, filter lengths were consistently 32 taps for the adaptive control filters and 120 taps for the fixed secondary path filters.

5 RESULTS

5.1 Synthesized Test Signals

Fig. 8 shows the noise reduction achieved at the frequencies selected for static ANC performance tests. Three measurements are shown at each frequency: the attenuation achieved at the error sensor location; the average attenuation at the 2 microphones near the operator's ears (the ear mics);

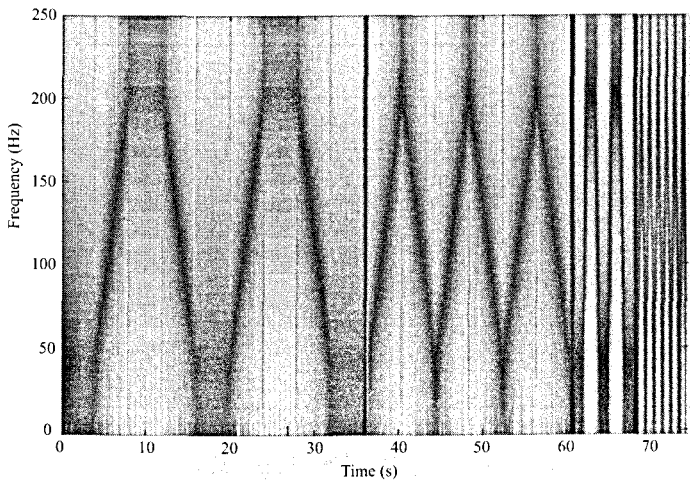

Fig. 7. Spectrogram of the swept sine excitation signal used to study dynamic ANC performance.

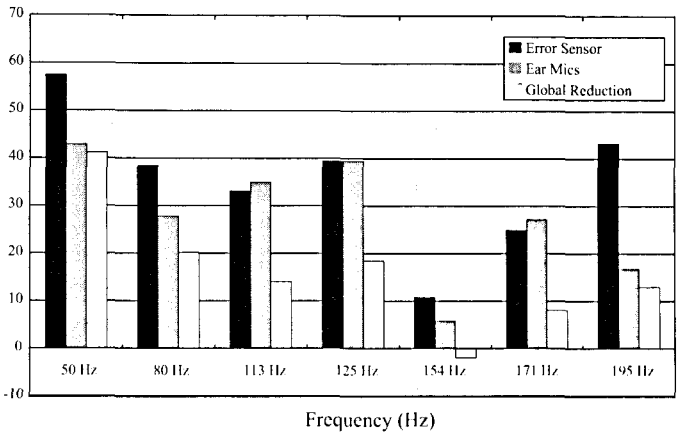

Fig. 8. Attenuation of static tones, comparing noise reduction achieved at various locations inside the cab.

and the spatially averaged attenuation (the global reduction), as recorded by the 12 microphones distributed throughout the upper half of the cab. The same 12 microphones were used in static noise tests using synthesized tones as well as recorded tractor noise. Average attenuation values were computed in pascals before being converted to dB values. At nearly all frequencies, reduction of the noise tone is significant throughout the cab. At 50 Hz, the amount of reduction at the error sensor is close to the dynamic range of the 12-bit analog-to-digital converters used in the control system electronics. Reduction throughout the rest of the cab is, on average, greater than 40 dB, which is to be expected due to the large wavelength of the low-frequency tone. The ED-based ANC system also performs well at high frequencies with a global reduction exceeding 10 dB at 195 Hz. The performance of the ANC system was diminished at 154 Hz, however, at which a single axial mode existed in the mock cab. The presence of an axial pressure mode should not have caused a problem for the energy density sensor, however. The cab sat in a rigid-walled hallway, and further investigation revealed that the hallway had several modes near 154 Hz, one of which was an axial mode between 154 and 155 Hz. It was found that the uncontrolled noise exhibited lower sound levels, by as much as 20 to 30 dB when compared to other frequencies, for nearly all observations. The lower uncontrolled noise levels, in addition to weak coupling between the control loudspeakers and the hallway modes, likely accounted for the poor results at this frequency.

Dynamic performance was recorded in terms of the amount of reduction in the equivalent sound level, L_{eq}, over the length of the test signal of interest. L_{eq} was measured with a flat frequency weighting. For dynamic measurements (with the synthesized test signal as well as recorded tractor noise), microphone signals were streamed to a computer hard disk for post processing. This allowed for accurate comparisons to

be made in L_{eq} over the duration of the test signal. However, at the time the dynamic measurements were made, only 4 of the 12 microphones distributed in the cab could be used for direct-to-disk recording. The 4 microphones chosen were the 4 closest to the front of the cab in the upper 6-microphone plane. The results obtained by the ANC system, using the previously described swept sine signal, are shown in Fig. 9. In the figure, "Global Reduction" refers to the spatially averaged reduction measured by 4 microphones rather than 12. The system tracked the changing noise signal well enough to achieve approximately 3 dB of global reduction in the Leq over the duration of the entire swept sine test signal as well as during each of its individual sections. The noise reduction at the error sensor often exceeded 4 dB and the average reduction seen by the ear mics even approached 5 dB. At all measurement locations, the system performance was nearly as good for the faster sweeps as it was for the slower sweeps. It should be noted that similar reductions in sound level were observed between the two ear mics in nearly all measurements.

A similar swept-sine excitation signal was also used to investigate the stability of the control system under different conditions of the cab door. For example, after measuring secondary path transfer functions with the cab door open, the controller was run with the door closed. In this case, the controller remained stable with a net reduction in the noise level, although the noise reduction achieved dropped by nearly 4 dB. Similarly, the controller performed well with the door open when the secondary paths were measured with the door closed, although performance was not as good as when the correct transfer functions were used.

5.2 Recorded Tractor Engine Noise

Attenuation of the tone corresponding to the tractor engine firing frequency for four different engine speeds appears in Fig. 10. Again, the best global reduction was seen at the lowest frequency. In this case, that frequency was 41 Hz, at which the global reduction exceeded 20 dB and was even slightly

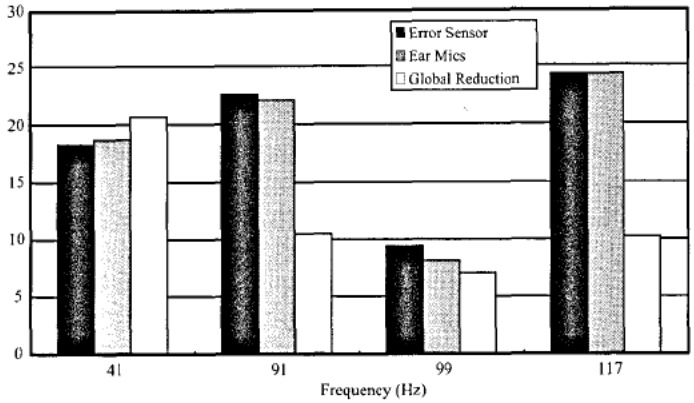

Fig. 10. Attenuation of static engine tones, comparing noise reduction achieved at various locations inside the cab.

better than the reduction at the error sensor or ear mics. For all tested engine speeds, the noise reduction at the ear mics was nearly equal to the noise reduction at the error sensor, which suggests that a good location was chosen for the placement of the ED-based error sensor. Even at the highest frequency of 117 Hz, over 10 dB of global reduction was achieved. The uncontrolled engine tone was much lower in amplitude at 99 Hz, which may explain the apparent reduction in ANC system performance at that frequency.

As mentioned previously, three different engine speed sweep rates were recorded for use in dynamic testing of the ANC system with recorded tractor noise. The fastest sweep was obtained by ramping up (and down) the engine speed of the tractor as fast as it would go. Fig. 11 shows the measured results for each of the three sweep rates. As the sweep rate

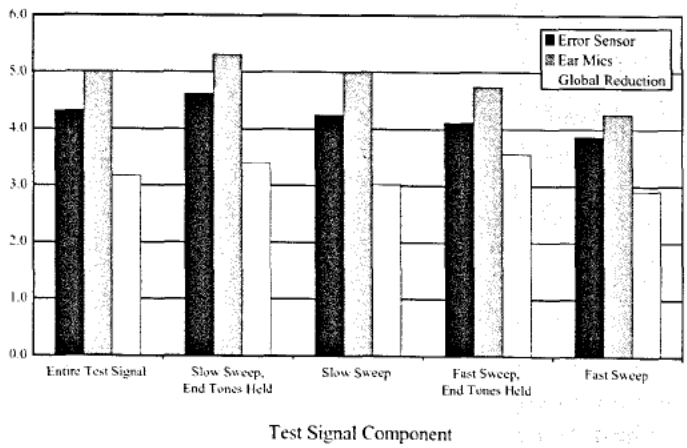

Fig. 9. Reduction in L_{eq} achieved during different sections of a dynamic test signal at various locations inside the cab.

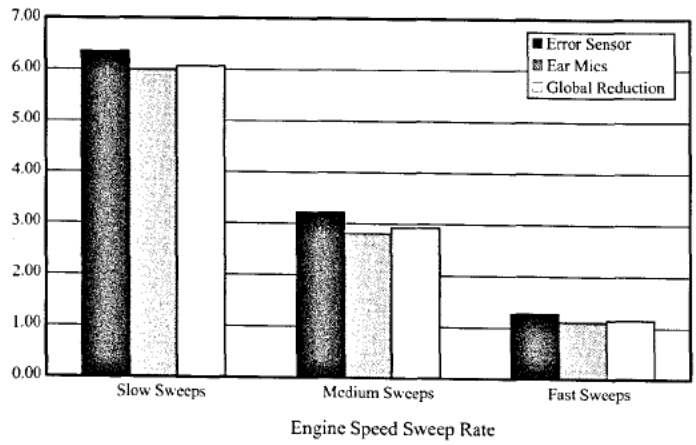

Fig. 11. Reduction in L_{eq} achieved during different recorded engine speed sweeps at various locations inside the cab.

increased, the amount of reduction in L_{eq} over the duration of the measurement decreased. At the slowest sweep rate, global reduction exceeded 6 dB. However, even at the fastest sweep rate, the system still achieved over 1 dB of reduction at all measurement locations (at *all* microphones, not just on average). These results suggest that the ED-based ANC system may reduce overall sound levels experienced in a tractor, even when the tractor is being operated through fast-paced work cycles in which engine speeds can vary rapidly.

Fig. 12 shows time-averaged spectra of the noise at the left ear microphone with and without ANC running. This example is for a slow engine speed sweep and shows that the ANC system was able to attenuate the engine tone throughout its entire frequency range (40 to 120 Hz).

6 CONCLUSIONS

Significant levels of noise reduction were achieved in the mock cabin, using the ED-based ANC system. Good global control was demonstrated in the cab with synthesized static and dynamic test signals as well as noise recorded from an actual tractor cab. The global nature of the control was apparent in all tests, except for one static test in which acoustic modes of the environment in which the cab was located may have adversely affected ANC system performance. These results suggest that at certain frequencies, the energy-based control system may indeed have some advantage over a similar pressure-based control system for this type of application. The advantages may be seen in that the ED-based system provides uniform control of the enclosed sound field over a relatively large frequency range (one for which acoustic modes of the enclosure are encountered) and the system is relatively insensitive to error sensor placement. Additionally, the system's ability to track recorded engine noise well enough to provide global noise reduction at the highest engine speed changes likely to be encountered suggests that such a system could potentially improve operating conditions and satisfy noise exposure standards in a real world environment.

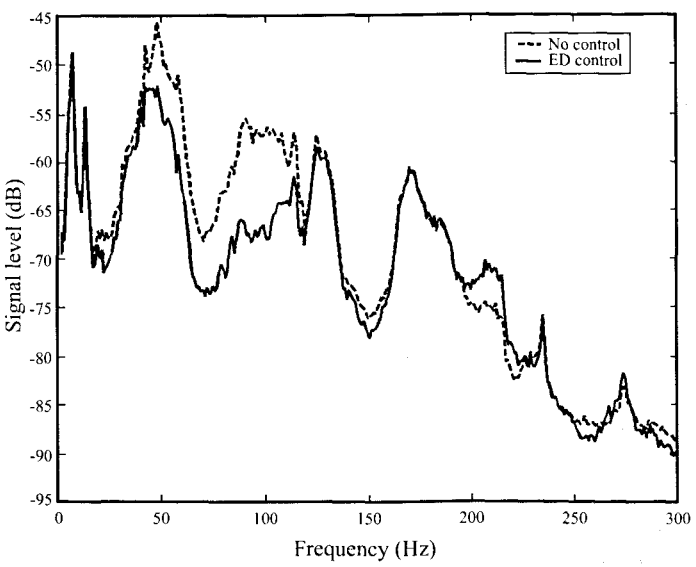

Fig. 12. Time-averaged spectrum of recorded engine noise, measured by the left ear microphone with and without ANC, using slow engine speed sweeps.

7 REFERENCES

[1] Y. Peng, A. Sasao, and S. Shibusawa, "Active noise control in proximity of a tractor operator's head," Trans. ASAE, **44**, 447-455 (2001).

[2] E. Carletti, D. Stanzial, and I. Vecchi, "Application of the active noise cancellation technique to earth-moving machines," Proc. Noise-93, St. Petersburg, Russia, May 31 – June 3, 1993, pp. 141-146.

[3] E. Carletti and I. Vecchi, "Reduction of noise inside cabs of earth-moving machines by active noise cancellation technique," Proc. Inter-Noise 94, Yokohama, Japan, Aug. 29-31, 1994, pp. 1417-1420.

[4] Ch. Carme, F. Fohr, and M. Besombes, "Active noise reduction in the cabin of an earth-moving machine," Proc. Inter-Noise 2002, Dearborn, Michigan, Aug. 19-21, (2002).

[5] E. Carletti, G. Miccoli, and I. Vecchi, "Earth-moving machine cab enclosed sound field active control simulation," Proc. Inter-Noise 96, Liverpool, U.K., July 30 - Aug. 2, 1996, pp. 1183-1186.

[6] J. W. Parkins, S. D. Sommerfeldt, and J. Tichy, "Narrowband and broadband active control in an enclosure using the acoustic energy density," J. Acoust. Soc. Am. **108**, 192-203 (2000).

[7] S. D. Sommerfeldt and P. J. Nashif, "An adaptive filtered-x algorithm for energy based active control," J. Acoust. Soc. Am. **96**, 300-306 (1994).

[8] J. W. Parkins, S. D. Sommerfeldt, and J. Tichy, "Error analysis of a practical energy density sensor," J. Acoust. Soc. Am. **108**, 211-222 (2000).

[9] J. W. Parkins, J. Tichy, and S. D. Sommerfeldt, "A comparison of two active control methods through an investigation of node structures," Proc. Active 99, Ft. Lauderdale, FL, Dec. 2-4, 1999, pp. 729-740.

[10] G. W. Elko, "An acoustic vector-field probe with calculable obstacle bias," Proc. Noise-Con 91, July, 1991, pp. 525–532.

[11] L. L. Locey and S. D. Sommerfeldt, "Analysis and comparison of three energy density probe designs," J. Acoust. Soc. Am. **114**, 2443 (2003).

Propagation constants from the response of a finite periodic beam

Venkata R. Sonti[a] and T.S.S. Narayana[b]

(Received 2005 March 05; revised 2006 February 01; accepted 2006 February 08)

An infinite periodic structure is usually modeled using a single span with appropriate periodic conditions. If a large finite periodic structure with N spans behaves like an infinite periodic structure, then, here also a single span model will suffice giving cost savings in computation. This paper is about such a meeting point between infinite and finite periodic structures. The propagation constant of an infinite periodically supported beam is obtained analytically from the response of a finite periodically supported beam. In an infinite periodic beam, e^g (g is the complex propagation constant) is the ratio of velocities in any two neighboring spans and is obtained using a single span model. Here, it is shown (analytically and experimentally) that if the finite periodic beam has enough spans, then e^g computed from the first two spans will match e^g for an infinite periodic beam in the attenuation zones.

Primary subject classification: 42; Secondary subject classification: 75

1 INTRODUCTION

Finite periodic structures such as railway tracks, bridges and ship hulls appear quite often in engineering. In literature, however, mostly infinite periodic structures have been theoretically investigated using wave propagation methods and more recently using FEM. Modeling of infinite periodicity is relatively simple. A single span or bay needs to be modeled and then periodicity imposed. Real structures being finite are not truly periodic and hence the structure has to be modeled in its totality. If the structure is large and has many degrees of freedom, solving for the response becomes computationally expense. Thus, it would be advantageous if under some conditions, a finite periodic structure would behave like an infinite structure. If that is so, once again, only a single span needs to be modeled. In this paper, we provide such a meeting ground where a finite periodic beam behaves like an infinite beam.

A distinct feature of infinite periodic structures is that they transmit vibrations in certain frequency bands (pass bands) and attenuate vibrations in other bands (stop bands). The ratio of velocities in the neighboring spans is e^g, where $g = a + ib$ is the propagation constant. The real part of g is the amplitude constant a and the imaginary part is b, the phase constant. Figures 1a and b show an infinite periodic beam and the corresponding amplitude constant a and phase constant b[1]. The regions where a is positive are the attenuation zones (or stop bands) and where it is zero are the propagation zones (or pass bands). Thus, there occur alternate frequency bands of attenuation and propagation.

In this paper, it is shown (using analysis and experiments) that the propagation constant g of an infinite periodically supported beam can be obtained using the response of a finite periodically supported beam. Provided the finite beam has enough spans, the ratio of velocities in the first two spans will be a good estimate for the value e^g of the corresponding infinite beam. The match between the two propagation constants will be close in the attenuation zones. In the propagation zones of the finite beam, its resonance behavior will show up.

Thus, a finite periodic structure looks like an infinite periodic structure from the two spans immediate to the driven span. And if one needs to know the frequencies which will be transmitted or attenuated from the excitation point, only a single span modeling needs to be performed (like in the infinite case).

There is another advantage. In an actual finite periodic structure, the supports differ from each other to within statistical bounds. Using the theory presented here, the propagation constant experimentally obtained from the finite structure corresponds to an overall support condition which can be mathematically identified. The identified mathematical support becomes the model for the finite as well as the infinite system.

Following the theoretical development, an experiment is conducted on a finite periodic beam (See Fig. 2). Frequency Response Functions (FRFs) which are ratios of the velocity response and the applied force Fourier transforms are obtained from a hammer impact test on the finite periodic beam and the ratio of the FRFs from the first two spans is used to obtain the propagation constant. A reasonable qualitative match is obtained with theory.

2 LITERATURE SURVEY

Dynamics of periodic structures have been studied using the linear matrix difference equations[2], the transfer matrix[3], the z-transform[4] and wave propagation methods[5-8]. Sen Gupta[9] presented a method to find resonance frequencies of finite periodic structures using the infinite periodic structure propagation constant. As part of finite structures, Mallik and Mead[10], Mallik and Murthy[11] and Murthy and Nigam[12] investigated the dynamics of homogenous rings. More complex systems such as layered rings were investigated by Reddy and Mallik[13,14].

[a] *Facility for Research in Technical Acoustics (FRITA), Department of Mechanical Engineering, Indian Institute of Science, Banglalore 560 012 INDIA; email: sonti@mecheng.iisc.ernet.in.*

[b] *Facility for Research in Technical Acoustics (FRITA), Department of Mechanical Engineering, Indian Institute of Science, Banglalore 560 012 INDIA*

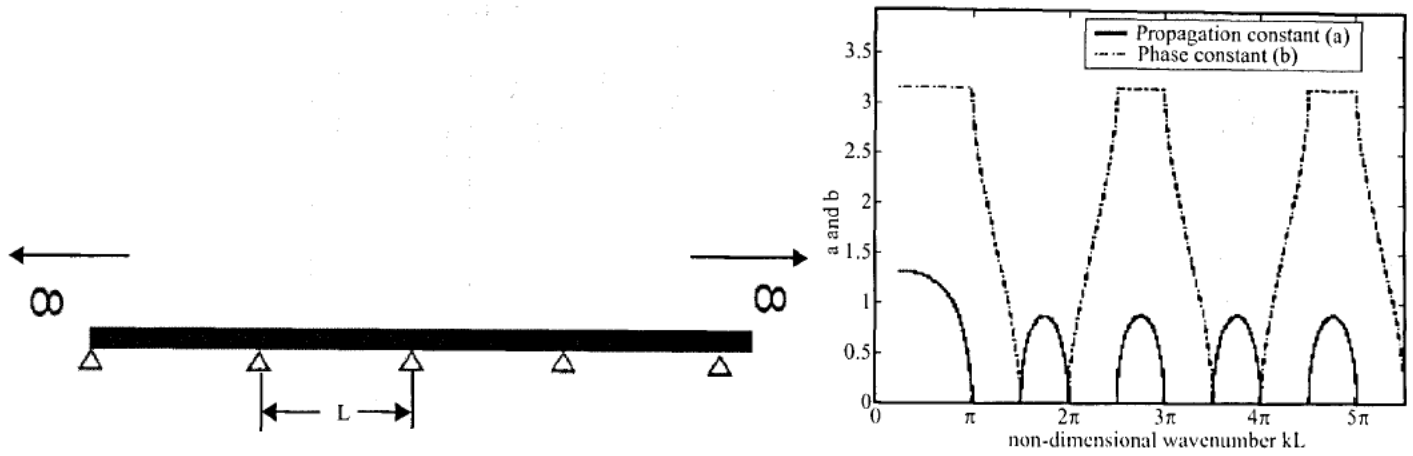

(a) (b)

Fig. 1. (a) Sketch of infinite periodic beam, (b) amplitude constant a and phase constant b from Euler theory.

3 THEORETICAL ANALYSIS

Figure 2 shows a 5-span-6-support beam with an overhang on the left. The span numbers and support numbers are given below the spans and supports, respectively. The span length is denoted by length L. It is assumed that all the supports in the periodic beam have t as the transmission coefficient and r as the reflection coefficient. The following derivation is based on Fig. 2.

If a wave of unit amplitude traveling to the right is incident on the fifth support, it will be transmitted into the fifth span as te^{-jKx} at the distance x to the right of the support. The constant j is $\sqrt{-1}$. At the sixth support (which is the last support) it will have an amplitude te^{-jKL}. If the sixth support has a reflection coefficient r_L, then the wave reflected from the support has an amplitude tr_Le^{-jKL} and travels towards the left (towards the fifth support). It reaches the fifth support and gets partly reflected into the fifth span and partly transmitted to the fourth span. The reflected wave has an amplitude trr_Le^{-2jKL} and the transmitted wave has an amplitude $t^2r_Le^{-2jKL}$. The reflected wave travels to the right and gets reflected at the sixth support as $trr_L^2e^{-3jKL}$. This wave travels to the left and at the fifth support gets reflected as $tr^2r_L^2e^{-4jKL}$ and transmitted as $t^2rr_L^2e^{-4jKL}$. This reflection and transmission will continue until a steady state condition is reached.

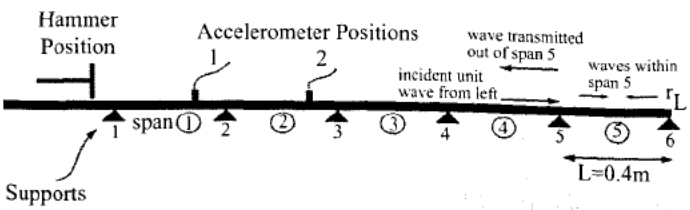

Fig. 2. The 5-span-6-support experimental setup with the hammer and accelerometer locations.

Thus, within the fifth span at a distance of x from the fifth support there is a train of right traveling waves (RTW) and a train of left traveling waves (LTW) given by

$$RTW = te^{-jKx} + trr_Le^{-2jKL}e^{-jKx} + tr^2r_L^2e^{-4jKL}e^{-jKx}... \quad (1)$$

$$LTW = tr_Le^{-2jKL}e^{jKx} + trr_L^2e^{-4jKL}e^{jKx} + tr^2r_L^3e^{-6jKL}e^{jKx}... \quad (2)$$

both of which form a geometric series with the common ratio given by rr_Le^{-2jKL}. Provided the magnitude of r is less than one, the two series can be summed and written as

$$RTW = \frac{te^{-jKx}}{1 - rr_Le^{-2jKL}} \quad (3)$$

$$LTW = \frac{tr_Le^{-2jKL}e^{jKx}}{1 - rr_Le^{-2jKL}} \quad (4)$$

The transmitted wave coming out of the fifth span (at the fifth support) is also a geometric series and is given by

$$W_{tr} = t^2r_Le^{-2jKL}\left[1 + rr_Le^{-2jKL} + r^2r_L^2e^{-4jKL}...\right] = \frac{t^2r_Le^{-2jKL}}{1 - rr_Le^{-2jKL}}$$

Thus, if a wave of amplitude A (instead of unity) is incident from the left onto the fifth support, the total wave reflected out of the fifth span is given by

$$W_{tot} = A\frac{t^2r_Le^{-2jKL}}{1 - rr_Le^{-2jKL}} + Ar,$$

where Ar is the reflection from the fifth support immediately after incidence (prior to transmission into the fifth span). Thus, the reflection coefficient of the total span number 5 as seen by a wave of amplitude A at the fifth support is given by

$$r_{L5} = \frac{t^2 r_L e^{-2jKL}}{1 - r r_L e^{-2jKL}} + r.$$

Similarly, for a wave incident from the left onto the fourth support, the entire beam to the right of the fourth support can be given by an equivalent reflection coefficient

$$r_{L4} = \frac{t^2 r_{L5} e^{-2jKL}}{1 - r r_{L5} e^{-2jKL}} + r.$$

And similarly for the third, second and first supports, the equivalent reflection coefficients are

$$r_{L3} = \frac{t^2 r_{L4} e^{-2jKL}}{1 - r r_{L4} e^{-2jKL}} + r$$

$$r_{L2} = \frac{t^2 r_{L3} e^{-2jKL}}{1 - r r_{L3} e^{-2jKL}} + r$$

$$r_{L1} = \frac{t^2 r_{L2} e^{-2jKL}}{1 - r r_{L2} e^{-2jKL}} + r,$$

respectively.

If a wave of unit amplitude traveling to the right is incident from the overhang portion onto the first support then the response within the first and second spans at the point $x = a$ within each span is given by

$$W_1 = \frac{t e^{-jKa}}{1 - r r_{L2} e^{-2jKL}} \left(1 + r_{L2} e^{-2jKL} e^{2jKa}\right)$$

and

$$W_2 = \frac{t e^{-jKL}}{1 - r r_{L2} e^{-2jKL}} \frac{t e^{-jKa}}{1 - r r_{L3} e^{-2jKL}} \left(1 + r_{L3} e^{-2jKL} e^{2jKa}\right),$$

respectively. The distance $x = a$ is measured within each span from its left support, i.e., for each span, $x = 0$ is at the left support of that span. Notice that the expression for W_2 has an extra term in front in comparison to W_1. This is the amplitude of the right traveling wave component in the first span incident on the second support.

The ratio of the two responses after canceling the common terms is given by

$$\frac{W_1}{W_2} = \frac{1 - r r_{L3} e^{-2jKL}}{t e^{-jKL}} \frac{1 + r_{L2} e^{-2jKL} e^{2jKa}}{1 + r_{L3} e^{-2jKL} e^{2jKa}} = e^g \qquad (5)$$

This ratio is a good estimate of e^g of the infinite beam where g is the complex propagation constant. Using the calculation above (Eqn. (5)), the amplitude constant a for the finite beam in Fig. 2 is shown in Fig. 3 with the curve for an infinite beam superimposed on it. The values of t and r for a simple support (which allows no vertical displacement, but allows rotation) are[15] $t = 0.5(1 - i)$ and $r = 0.5(1 + i)$. Here, $r_L = -1$ for the beam shown in Fig. 2. As can be seen, in the attenuation zones both the curves match closely. This match will occur provided the finite beam has at least 5 or 6 spans and the ratio of responses from the first and second span will give the best

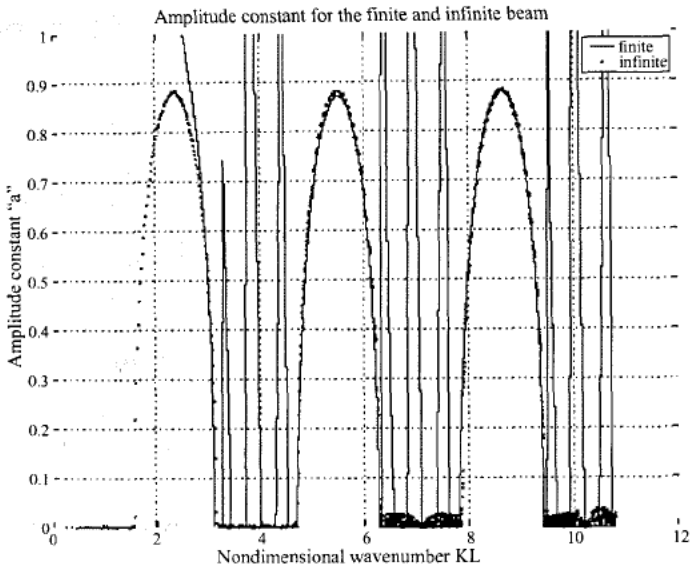

Fig. 3. Comparison of amplitude constants between an infinite and a finite periodic beam.

result. It is important to leave out the overhang portion where excitation is given and hence is not part of the periodicity. It may be noted that although e^g is obtained (analytically or experimentally), the amplitude constant a is of main interest. The phase constant b is known once the values of a in the attenuation zone are known.

In Fig. 4, a plot of a from W_4/W_5 is compared against that obtained from W_1/W_2 (Eqn. (5)). The inaccuracy in using the fourth and fifth spans is evident.

The reason for this inaccuracy can be seen in Eqn. (5). The r_L's become equal to each other within the attenuation zones as one proceeds more and more to the left from the fifth span to the overhang which is the source of excitation. Physically, as the number of spans increases beyond a certain value, the beam looks almost infinite from the overhang side (except in the propagation zones where the number of resonances keep increasing). The attenuation value reaches a saturation value. This can be verified by plotting all of the r_L's. Since r_{L2} and r_{L3} are almost equal in the attenuation zone, the second ratio in Eqn. (5) cancels out and even in the remaining ratio we replace r_{L3} with r_{L2} and write

$$\frac{W_1}{W_2} = \frac{1 - r r_{L2} e^{-2jKL}}{t e^{-jKL}}. \qquad (6)$$

The above expression is a very good approximation to e^g (and a) of the infinite beam in the attenuation zones. (The value of a in the propagation zones is zero for the infinite beam). It even has the $1/t$ dependence as given in Ref. [1].

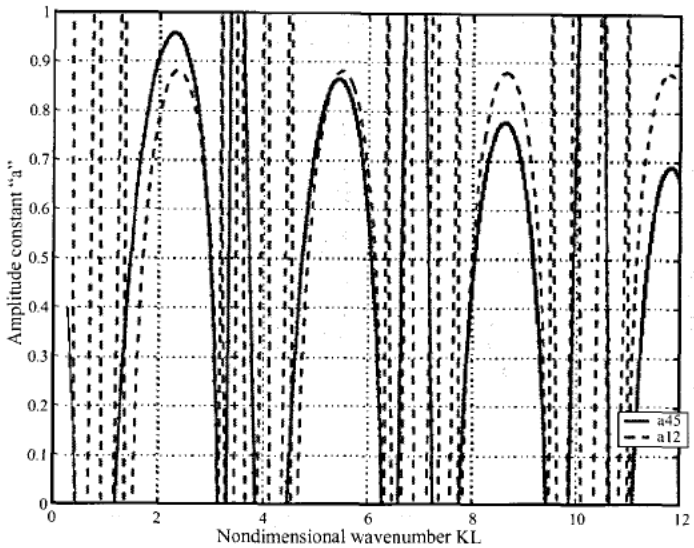

Fig. 4. Comparison of amplitude constants using the response from the first two spans (a12) and the last two spans (a45) in a finite periodic beam.

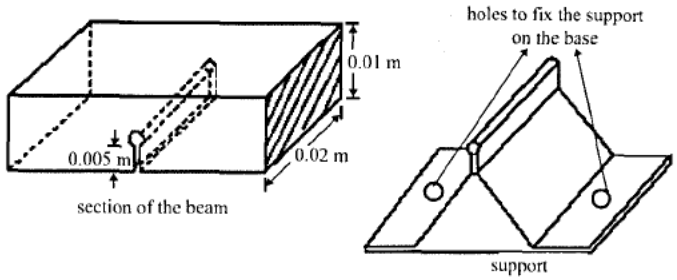

Fig. 5. Schematic of a "simple support".

4 EXPERIMENTS WITH A 5-SPAN-6-SUPPORT BEAM

4.1 The Setup and Measurements

The experimental setup consists of a five span aluminum beam with six supports as shown in Fig. 2. Each span is 40 cm long. There is an overhang 40 cm long on the left side. The excitation is given in this overhang portion of the beam. Each support is constructed to behave like a simple support, i.e., the vertical motion at the support is arrested and the rotation is allowed (as shown in Fig. 5). A groove is cut into the underside of the beam, such that a corresponding section of the support snugly fits into it. The top part of the groove is cylindrical and so is that of the inserted part of the support. The supports are then bolted to a heavy iron block forming the base. The experimental results, however, show that this support does deviate from the intended simple-support behavior. The experimental beam properties are given in Table 1.

Table 1 – Material and geometric properties of the aluminum beam

Youngs Modulus	ρ	μ	thickness	width
62e9 N/m^2	2699 Kg/m^3	0.3	0.01 m	0.02 m

The beam is excited with an impact hammer (B&K Type 8210) at a distance of 7.5 cm to the left of the first support from the free end. The mobility measurements (made with two accelerometers B&K Type 4508) are taken at 8.5 cm left of the second support and 8.5 cm left of the third support as shown in Fig. 2 and 20 averages are taken in arriving at the final mobility FRFs. Coherence function is used to ascertain the quality of the measurement. A multi-channel Pulse (B&K Type 2885) was used to obtain the two mobility FRFs simultaneously and the propagation constant is then computed from these FRFs.

If the two FRFs are given as

$$FRF_1 = \frac{v_1(\omega)}{F(\omega)} \text{ and } FRF_2 = \frac{v_2(\omega)}{F(\omega)},$$

where $v_1(\omega)$ and $v_2(\omega)$ are the velocity spectra at the accelerometers 1 and 2, and $F(\omega)$ is the spectrum of the force, then the propagation constant $g = a + jb$ is given by[1]

$$e^g = \frac{FRF_1}{FRF_2}.$$

The amplitude constant a is then given by[1]

$$a = \log\left(\left|e^g\right|\right).$$

The above result is for a finite beam. However, as mentioned earlier, the ratio of velocities from the first two spans has attenuation zones closely approximating that of an infinite beam as shown in Fig. 3. The propagation zones have a complex behavior due to the resonance of the finite periodic beam. Thus, one can find the propagation constant g (hence a) of the infinite beam using that of the finite beam. In the attenuation zone (which is typically of interest), it exactly resembles the infinite beam and in the propagation zones the infinite beam has zero values for a.

4.2 Results

The two frequency response functions (at the two accelerometer positions) are shown in Fig. 6. The left figure is for accelerometer 1 and the right for accelerometer 2. The typical periodic structure behavior can be seen where sets of resonances are separated by a long antiresonance zone